

# On-Chip Dispersion Measurement of the Quadratic Electro-Optic Effect in Nonlinear Optical Polymers Using a Photonic Integrated Circuit Technology

Volume 11, Number 3, June 2019

Patrick Steglich, *Member, IEEE*

Claus Villringer

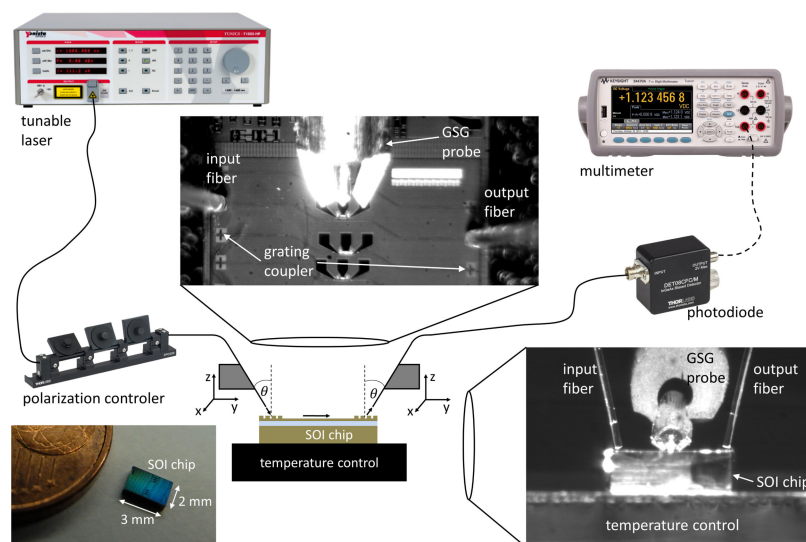
Birgit Dietzel

Christian Mai

Sigurd Schrader

Mauro Casalboni

Andreas Mai, *Member, IEEE*



DOI: 10.1109/JPHOT.2019.2917665

# On-Chip Dispersion Measurement of the Quadratic Electro-Optic Effect in Nonlinear Optical Polymers Using a Photonic Integrated Circuit Technology

Patrick Steglich ,<sup>1,2</sup> Member, IEEE, Claus Villringer,<sup>2</sup> Birgit Dietzel,<sup>2</sup> Christian Mai,<sup>1</sup> Sigurd Schrader,<sup>2</sup> Mauro Casalboni,<sup>3</sup> and Andreas Mai ,<sup>1,2</sup> Member, IEEE

<sup>1</sup>IHP - Leibniz-Institut für innovative Mikroelektronik, Frankfurt(Oder) D-15236, Germany

<sup>2</sup>Technical University of Applied Sciences Wildau, Wildau D-15745, Germany

<sup>3</sup>University of Rome "Tor Vergata", Rome I-00133, Italy

DOI:10.1109/JPHOT.2019.2917665

This work is licensed under a Creative Commons Attribution 3.0 License. For more information, see <https://creativecommons.org/licenses/by/3.0/>

Manuscript received April 12, 2019; revised May 10, 2019; accepted May 14, 2019. Date of publication May 20, 2019; date of current version May 29, 2019. This work was supported in part by the European Regional Development Fund (10.13039/501100008530) and in part by the German Research Foundation and the Open Access Publication Funds of the TH Wildau. Corresponding author: Patrick Steglich (e-mail: patrick.steglich@th-wildau.de).

**Abstract:** A novel method to determine the dispersion of the quadratic electro-optic effect in nonlinear optical materials by using a silicon-on-insulator microring resonator is presented. The microring consists of a silicon slot waveguide enabling large dc electric field strength at low applied voltages. The dispersion of third-order hyperpolarizability of a linear conjugated dye is approximated by using a two-level model for the off-resonant spectral region. As an example, the dispersion of the resonance wavelength of the resonator filled with a dye doped polymer was measured in dependence of the applied dc voltage. The polymer was poly (methylmethacrylate) doped with 5 wt% disperse red 1 (DR1), and the measurements have been carried out at the telecommunication wavelength band around 1550 nm (optical C-band). The described measurements represent a new technique to determine the dispersion of the third-order susceptibility and molecular hyperpolarizability of the material filled into the slot of the ring-resonator.

**Index Terms:** Electro-optical devices, nonlinear optics, integrated optics, integrated optics materials, optical materials, integrated optics devices, polymer active devices.

## 1. Introduction

Recent developments in the field of silicon-organic hybrid (SOH) devices [1]–[4] have led to a renewed interest in nonlinear optical (NLO) organic materials [5]. SOH modulators exhibit large bandwidth [6], low-power consumption [7] and typically take advantage of electro-optical (EO) effects in the off-resonant regime [8], which enables the generation of higher order modulation formats since amplitude and phase can be manipulated independently from each other. Usually, there are two EO effects of practical importance, namely the Pockels-effect (linear EO effect) and the DC Kerr-effect (quadratic EO effect). The quadratic EO effect is significantly weaker compared to the linear EO effects but it does not require the lack of centrosymmetry of the system. Moreover, it was demonstrated that the quadratic EO effect is very attractive due to its inherent long-term and thermal

stability compared to the linear EO effect in polymers [9], [10] and its potential high bandwidth [11]. One major advantage of third-order nonlinear optical polymers is that they exhibit the quadratic EO effect as well as the all-optical Kerr-effect at the same time, leading to completely new device concepts; e.g. electrically controlled multistable switches [12]. Latest research on slot waveguide-based devices has shown the feasibility of the quadratic EO effect for on-chip applications at voltages as low as 1 V [13], which demonstrates the compatibility with typical complementary metal-oxide semiconductor (CMOS)-driver voltages. A first RF modulator solely based on the quadratic EO effect in a SOH ring resonator has been demonstrated recently [14]. Because of such innovative device concepts, the quadratic EO effect in SOH slot waveguides is expected to be an emerging technology for on-chip photonic circuits. For the optimization of such devices, the control of dispersion of the quadratic EO effect is crucial.

In literature, different findings about EO properties measured in bulk films and those measured on-chip are reported [8], [15], [16]. Moreover, all reported values are measured at single wavelengths so far. Therefore, a method to infer the dispersion of the quadratic EO effect in polymers directly from the measured on-chip performance is beneficial to avoid such discrepancies and to support simulation studies of integrated optical devices with reliable information.

In this work, we present a method to determine the dispersion of the quadratic EO effect of NLO materials by using a silicon micro-ring resonator. The ring resonator comprises a slot waveguide and is fabricated by CMOS-compatible processes. In this way, the on-chip performance of novel EO materials can be determined using the same technological conditions as for the final device.

## 2. Theory

The quadratic EO effect describes the field induced optical anisotropy described by the change of an ordinary and extraordinary refractive index component corresponding to  $\Delta n_o$  and  $\Delta n_e$ , respectively. The indicatrix

$$a_{11}x^2 + a_{22}y^2 + a_{33}z^2 + 2a_{23}yz + 2a_{31}zx + 2a_{12}yx = 1 \quad (1)$$

is related to the quadratic EO coefficients of an isotropic material as

$$\begin{bmatrix} a_{11} - \frac{1}{n_\omega} \\ a_{22} - \frac{1}{n_\omega} \\ a_{33} - \frac{1}{n_\omega} \\ a_{23} \\ a_{31} \\ a_{12} \end{bmatrix} = \begin{bmatrix} R_{11} & R_{12} & R_{12} & 0 & 0 & 0 \\ R_{12} & R_{11} & R_{12} & 0 & 0 & 0 \\ R_{12} & R_{12} & R_{11} & 0 & 0 & 0 \\ 0 & 0 & 0 & \frac{1}{2}(R_{11} - R_{12}) & 0 & 0 \\ 0 & 0 & 0 & 0 & \frac{1}{2}(R_{11} - R_{12}) & 0 \\ 0 & 0 & 0 & 0 & 0 & \frac{1}{2}(R_{11} - R_{12}) \end{bmatrix} \begin{bmatrix} E_x^2 \\ E_y^2 \\ E_z^2 \\ E_y E_z \\ E_z E_x \\ E_x E_y \end{bmatrix}. \quad (2)$$

At the presence of an electric field in x-direction ( $E_x$ ) and assuming a small change of the refractive index, the indicatrix can be approximated as

$$\frac{x^2}{(n_\omega - \frac{1}{2}n_\omega^3 R_{11} E_x^2)^2} + \frac{y^2 + z^2}{(n_\omega - \frac{1}{2}n_\omega^3 R_{12} E_x^2)^2} = 1, \quad (3)$$

where  $n_\omega$  is the refractive index of the organic material at the optical frequency.  $R_{11}$  and  $R_{12}$  are the quadratic EO coefficients. Then, the change of extraordinary and ordinary refractive index are determined by [17]

$$\Delta n_e = -\frac{1}{2}n_\omega^3 R_{11} E_x^2 = \frac{1}{n_\omega} \frac{3}{2} \chi_{3333}^{(3)}(-\omega; \omega, 0, 0) E_x^2 \quad (4)$$

and

$$\Delta n_o = -\frac{1}{2}n_\omega^3 R_{12} E_x^2 = \frac{1}{n_\omega} \frac{3}{2} \chi_{1133}^{(3)}(-\omega; \omega, 0, 0) E_x^2, \quad (5)$$

where  $\omega = 2\pi c/\lambda$ ,  $\chi_{3333}^{(3)}(-\omega; \omega, 0, 0)$  and  $\chi_{1133}^{(3)}(-\omega; \omega, 0, 0)$  represent the third-order susceptibility tensor elements. Consequently, there exists the following relations

$$R_{11} = -\frac{3}{n_\omega^4} \chi_{3333}^{(3)}(-\omega; \omega, 0, 0), \quad (6)$$

$$R_{12} = -\frac{3}{n_\omega^4} \chi_{1133}^{(3)}(-\omega; \omega, 0, 0). \quad (7)$$

The third-order susceptibility tensor elements  $\chi_{1133}^{(3)}(-\omega; \omega, 0, 0)$  and  $\chi_{3333}^{(3)}(-\omega; \omega, 0, 0)$  are related to the molecular third-order hyperpolarizability  $\gamma(-\omega; \omega, 0, 0)$  by [17]–[19]

$$\chi_{1133}^{(3)}(-\omega; \omega, 0, 0) = \frac{1}{15} N f_\omega^2 f_0^2 \gamma(-\omega; \omega, 0, 0), \quad (8)$$

$$\chi_{3333}^{(3)}(-\omega; \omega, 0, 0) = \frac{1}{5} N f_\omega^2 f_0^2 \gamma(-\omega; \omega, 0, 0), \quad (9)$$

where  $N$  is the number of molecules per unit volume,  $f_\omega$  and  $f_0$  are dimensionless local-field correction factors at the optical frequency  $\omega$  and at a static electric field ( $\omega = 0$ ), respectively. The local-field correction factor at optical frequencies is described by the Lorentz expression  $f_\omega = (n_\omega^2 + 2)/3$  whereas the local-field correction factor at a static electric field is described by the Onsager expression  $f_0 = \epsilon(0)(n_\omega^2 + 2)/[n_\omega^2 + 2\epsilon(0)]$ , where  $\epsilon(0)$  is the static dielectric constant of the organic material.

A multilevel model that use adjustable parameters to fit the data or results of semi-empirical calculations that cannot be directly validated by experiment is typically used to describe the dispersion of the third-order hyperpolarizability near to the first resonance [20]. However, a two-level model for a nonpolar ground state and polar excited state can adequately describe the dispersion of the third-order hyperpolarizability far from the first resonance. The two-level model in the off-resonant region is expressed by [17], [21]

$$\gamma(-\omega; \omega, 0, 0) = \frac{\zeta_{01}}{(\omega_0 - \omega)^3} + \frac{\zeta_{02}}{(\omega_0 - \omega)^2} + \frac{\zeta_{03}}{(\omega_0 - \omega)}. \quad (10)$$

Here,  $\zeta_{01}$ ,  $\zeta_{02}$  and  $\zeta_{03}$  are frequency-independent constants and  $\omega_0$  represents the first resonant frequency of the molecule. Note that in case when the applied electric field is modulated, the modulation frequency will not occur in the denominators of Eq. (10) because it is small compared to the optical frequencies and, hence, will be neglected [17]. Inserting Eq. (10) into Eq. (8) and 9 and substituting the result in Eq. (6) and (7) yields the expressions for the dispersion of the quadratic EO coefficients given by

$$R_{11} = -\frac{1}{15} \left[ \frac{(n_\omega^2 + 2)^2}{n_\omega^4 + 2n_\omega^2 \epsilon(0)} \right]^2 \left[ \frac{A}{(\omega_0 - \omega)^3} + \frac{B}{(\omega_0 - \omega)^2} + \frac{C}{(\omega_0 - \omega)} \right], \quad (11)$$

$$R_{12} = -\frac{1}{45} \left[ \frac{(n_\omega^2 + 2)^2}{n_\omega^4 + 2n_\omega^2 \epsilon(0)} \right]^2 \left[ \frac{A}{(\omega_0 - \omega)^3} + \frac{B}{(\omega_0 - \omega)^2} + \frac{C}{(\omega_0 - \omega)} \right], \quad (12)$$

where  $A = N\epsilon(0)^2\zeta_{01}$ ,  $B = N\epsilon(0)^2\zeta_{02}$  and  $C = N\epsilon(0)^2\zeta_{03}$  are constant in frequency. This model has been applied to measure the dispersion of the quadratic EO effect in bulk polymers achieved using the prism coupling technique [21]. In the following, we employ this model to measure the the quadratic EO effect using an integrated ring resonator for the evaluation of the in-device performance.

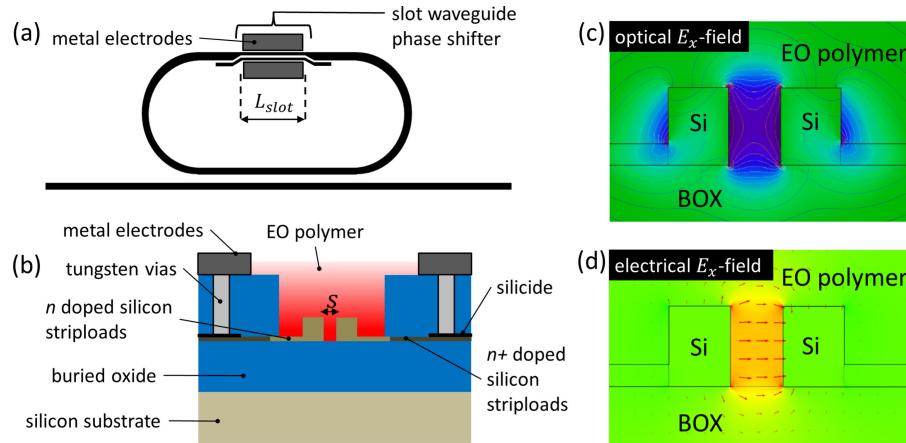


Fig. 1. (a) Geometry of the micro-ring resonator. The slot waveguide is partially introduced to the ring. (b) Cross-sectional view of the slot waveguide. (c) Simulated optical field (TE-mode) and (d) electrical field inside the slot waveguide. Adopted from Ref. [14].

### 3. Experiment

The micro-ring resonator, as schematically shown in Fig. 1(a), was fabricated on a 200 nm silicon-on-insulator wafer using a photonic integrated circuit (PIC)-technology as a modular part of a complex electronic-photonic integrated circuit (EPIC)-SiGe-BiCMOS platform [22]. The PIC-technology enables the fabrication of silicon-based ring resonators together with conductive silicon bridges connecting metal electrodes to the slot waveguide (Fig. 1(b)). The ring geometry, device performance and details on the fabrication process can be found in our previous work [14], [23], [24]. The slot waveguide allows an enhanced optical field confinement in between the two silicon rails [25], as shown in Fig. 1(c). An electric field inside the slot (Fig. 1(d)) is induced by applying a voltage to the metal electrodes. A more comprehensive description of such CMOS-compatible slot waveguide design can be found in Refs. [26], [27]. In particular, a simulation study of slot waveguides comprising the same EO polymer as in the present work can be found in Ref. [28].

Here, we employ the linear conjugated dye disperse red 1 (DR1) doped into a poly(methyl methacrylate) (PMMA) matrix from SigmaAldrich (344206 Aldrich and 445746 Aldrich) as cladding material. The dye is composed of a conjugated chain of  $\pi$ -bounds with donor-acceptor polar groups at the ends, yielding a large linear EO effect when aligned through a poling procedure, but also a significant quadratic EO effect in any molecular order. Such conjugated dyes provide a large quadratic EO effect due to their delocalized  $\pi$ -electron system. The sample preparation was carried out as follows. The DR1 dye is co-dissolved with PMMA in 1,1,2,2-tetrachlorethane. We have prepared a 60 g/l polymer-solution having a 5 wt% dye concentration. The polymer-solution is deposited on the chip in a post-process using the spin-coating technique. Afterwards, the samples were dried in a vacuum oven to remove the solvent.

Additionally, we have prepared thin films (500 nm) of the guest-host system DR1/PMMA on glass and silicon substrates to obtain the linear optical properties. The inset of Fig. 2 shows the structural formula of DR1 and PMMA. The dispersion of the refractive index  $n_\omega$  and of the extinction coefficient  $\kappa$  is measured by means of spectroscopic ellipsometry (Sentech SE 850). Spectral photometry (PerkinElmer Lambda 1050) were performed to support the ellipsometric analysis. The layer was modelled as a mixture of DR1 and PMMA using the Bruggemann effective medium approximation. For the non-absorbing PMMA matrix, a Sellmeier model was employed whereas for the DR1 portion a Tauc-Lorentz oscillator was used. The results are plotted in Fig. 2. From the spectrum of Fig. 2 we infer the first resonant wavelength of 521.6 nm and a cut-off wavelength of  $\lambda_{cut-off} = 645.5$  nm. The extinction coefficient  $\kappa$  becomes zero if  $\lambda > \lambda_{cut-off}$ . Note, the quadratic EO effect is enhanced at wavelengths near the first resonant wavelength peak ( $\omega \rightarrow \omega_0$ ). However, a

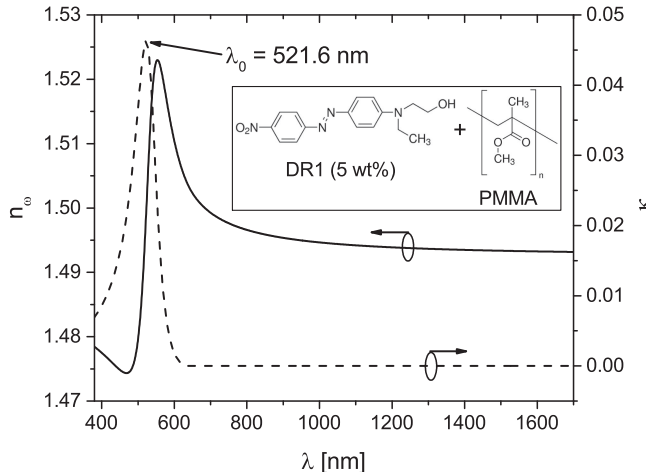


Fig. 2. Dispersion of the refractive index  $n_\omega$  and of the extinction coefficient  $\kappa$  of the guest-host system DR1/PMMA. The spectrum of the extinction coefficient shows a good transparency in the optical C-band and a first resonant peak at 521.6 nm. Inset: Chemical structures of the employed EO dye disperse red 1 (DR1) and of the polymer matrix, which consists of poly(methyl methacrylate) (PMMA).

low absorption is required to guarantee high quality data transfer for many applications in telecommunications. This is only possible in the off-resonant spectral region; i.e. far away from the cut-off wavelength. A typical communication band is the optical C-band (1530 nm – 1565 nm), where the polymer as well as silicon are highly transparent and exhibit a low refractive index dispersion. Consequently, our analysis is focused on this wavelength region. From Fig. 2 it is apparent that the refractive index dispersion of the utilized polymer is low and, hence, the dispersion of the quadratic EO coefficients  $R_{11}$  and  $R_{12}$  are dominated by the term in the second square brackets in Eq. (11) and Eq. (12), respectively.

In the experimental set-up for measurements of the transmission spectra of the ring resonator, as shown in Fig. 3, a tunable external cavity laser (Yenista TUNICS T100S-HP) serves as light source. The tunable laser is used to scan the wavelength dependent behavior of the ring resonator. A fiber-grating-coupler set-up is used to couple the light into the chip. The laser is connected to the input fiber, while a fiber coupled InGaAs photodetector (Thorlabs DET08CFC/M) is connected to the output fiber. Due to the polarization dependence of the grating coupler, the polarization of the input light was adjusted in such a way that highest transmission is achieved by using a paddle style fiber polarization rotator (Thorlabs FPC031). The ground-signal-ground (GSG) electrodes on the chip are connected to an electric power source (Keysight Sourcemeter 2400) through tungsten DC probes (Picoprobes A 40A-GSG-150-P). Please note that the resonance peak position of the ring resonator is strongly temperature dependent due to the relatively large thermo-optic effect in silicon. We have measured a temperature shift of about 81 pm/ $^\circ\text{C}$ . Therefore, the chip was temperature controlled and stabilized at 35  $^\circ\text{C}$ .

Applying a voltage to the GSG electrodes induces an electric field inside the slot waveguide. In our experiment, the electric field of the guided optical wave is collinear with the applied electrical field. Therefore, we measure the dispersion of the  $R_{12}$  component and evaluate the  $R_{11}$  component as well as the Kerr coefficient  $K$  using the same fitting parameter  $A$ ,  $B$  and  $C$ .

The applied electric field, however, leads to a refractive index change of the polymer given by Eq. (5). As a consequence, the resonance wavelength is shifted because the resonance condition is changed due to a change of the optical path length. This resonance wavelength shift as function of the applied voltage can be described by [13]

$$\Delta\lambda = \frac{1}{n_\omega} \frac{3}{2} \chi_{3333}^{(3)}(-\omega; \omega, 0, 0) \frac{U_{DC}^2}{s^2} L_{slot} \Gamma_{slot}, \quad (13)$$

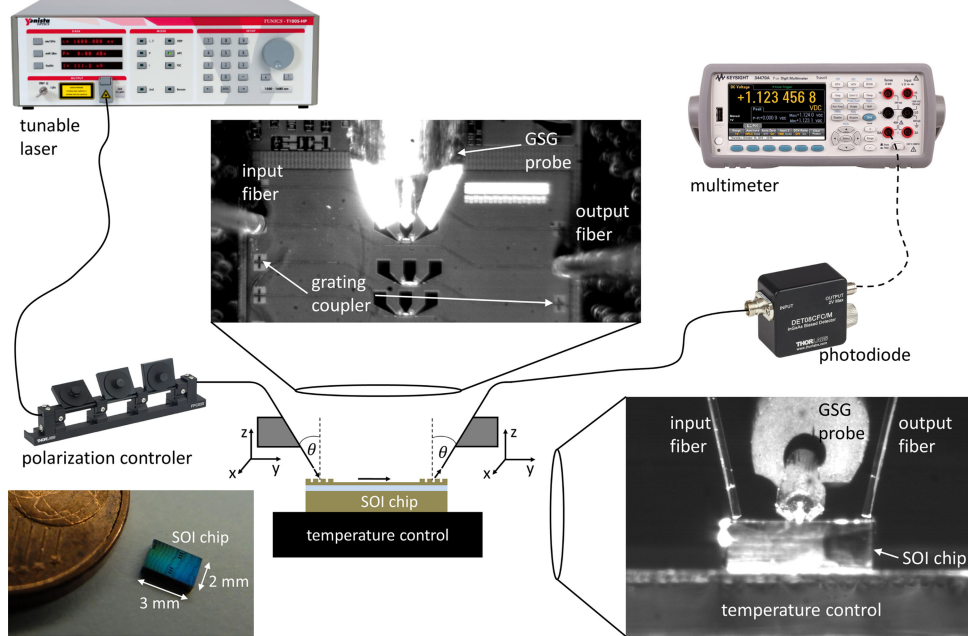


Fig. 3. Schematic of the experimental setup. The light of an external cavity laser is polarized and coupled into the silicon-on-insulator (SOI) chip by means of vertical fiber couplers. The light transmitted through the sample is coupled back to a fiber and recorded with an InGaAs photodiode. The sample holder is temperature controlled and the SOI chip is connected through tungsten DC probes to an electric DC source.

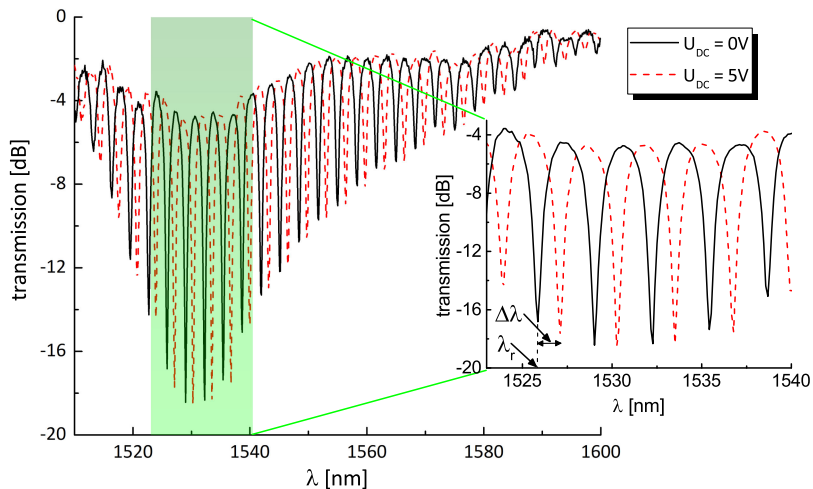


Fig. 4. Spectra of the micro-ring resonator at zero voltage (black solid line). The resonance peaks are red-shifted (red dashed line) after applying a DC voltage of 5 V.

where  $U_{DC}$  is the applied DC voltage,  $s$  is the slot width,  $L_{slot}$  is the slot waveguide length and  $\Gamma_{slot}$  is the confinement factor of the slot waveguide. Note that we have used the approximation  $E_x = U_{DC}/s$ . First, the transmission spectrum of the micro-ring resonator was measured at several voltages. Fig. 4 shows the obtained spectrum at 0 V and 5 V. From Fig. 4 it can be seen that the resonance peaks are red shifted (red dotted line) after applying a voltage. This shift is larger for smaller wavelengths due to the dispersion of the quadratic EO effect. Hence, it is straightforward to calculate the quadratic EO coefficient  $R_{11}$  at each resonance peak to get the dispersion. Therefore,

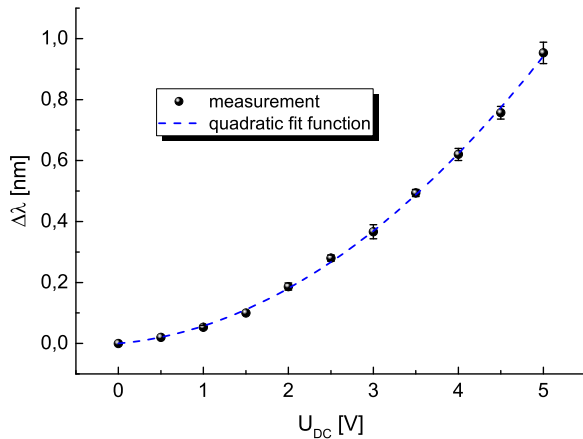


Fig. 5. Resonance wavelength shift as function of the applied DC voltage. The resonance wavelength at 0 V was 1549.8 nm.

in a second step we plotted for each resonance peak the shift  $\Delta\lambda$  as function of the applied voltage ranging from 0 V to 5 V in 0.5 V steps. Fig. 5 shows exemplary one plot of the resonance wavelength shift  $\Delta\lambda$  as function of the voltage  $U_{DC}$  for a resonance peak at 1549.8 nm. It is apparent from this fig., when the applied voltage  $U_{DC}$  varies linearly the wavelength shift  $\Delta\lambda$  varies quadratically. We applied a quadratic fit function  $\Delta\lambda = M U_{DC}^2$  to each graph (for each resonance peak), where  $M$  is a constant obtained from a least square fit procedure.

Then, a coefficient comparison between the quadratic fit function and Eq. (13) yields the third-order susceptibility component

$$\chi_{3333}^{(3)}(-\omega; \omega, 0, 0) = \frac{2n_\omega s^2 M}{3L_{slot} \Gamma_{slot}}. \quad (14)$$

Putting Eq. (14) into Eq. (6) gives the quadratic EO coefficient  $R_{11}$  for each resonance peak within our measurement range. To obtain the fitting constants  $A$ ,  $B$  and  $C$  we have applied a least square fit to the experimental data using Eq. (11). Once we have deduced these fitting constants from the dispersion of  $R_{11}$ , it is possible to determine the dispersion of  $R_{12}$  since the fitting constants are included in Eq. (11) as well as in Eq. (12).

#### 4. Results and Discussion

Fig. 6 shows the measured dispersion of  $R_{11}$  in the optical C-band and the fitted curve. The fitting curve in Fig. 6 is in good agreement with experimental data and is extended to the optical O-band. The following fitting constants are used:

$$A = N\epsilon(0)^2 \zeta_{01} = -7, 94 \cdot 10^{27} \quad (15)$$

$$B = N\epsilon(0)^2 \zeta_{02} = 1, 34 \cdot 10^{28} \quad (16)$$

$$C = N\epsilon(0)^2 \zeta_{03} = -1, 53 \cdot 10^{28} \quad (17)$$

The coefficient of determination is  $R^2 = 0.99998$  and the residual sum of squares is  $8.82814 \cdot 10^{-5}$ , reflecting the high accuracy of the least square fit. It is worth to mention that although the presented ring resonator shows an excellent performance in terms of resonance wavelength shift as function of the applied voltage, future devices could employ slot waveguides with smaller gaps to increase the EO efficiency.

The optical O-band around 1310 nm is beside the optical C-band the most important communication wavelength range. Our method provides reliable information for the communication wavelengths

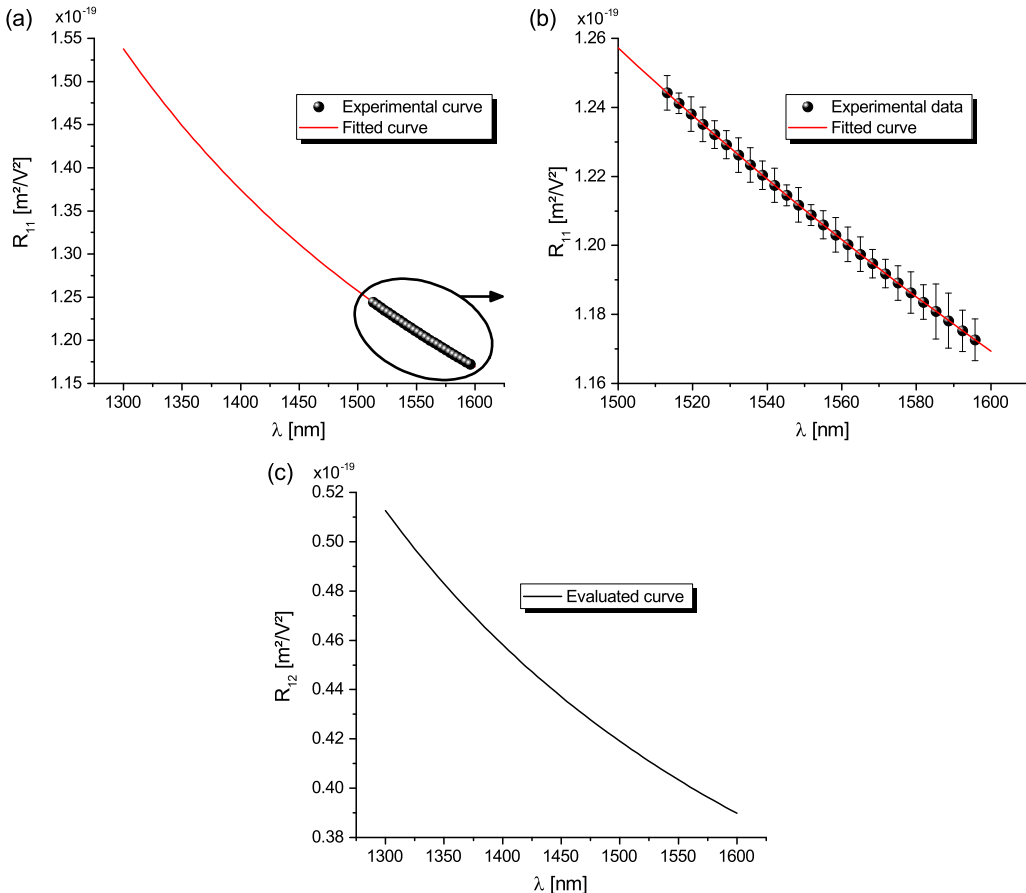


Fig. 6. Dispersion of the quadratic EO coefficients. (a) The values of  $R_{11}$  are deduced from experimental data (b) and fitted. (c) The values for  $R_{12}$  are evaluated using the values of  $R_{11}$  under the assumption of a two-level model and that electronic mechanisms are dominating in the off-resonant spectral region.

1310 nm and 1550 nm and, hence, supporting simulation studies of EO devices. The observed dispersion and, in particular, the fitting curve reasonably fit with literature data for bulk polymers, as it has been measured with the prism coupling technique [21]. We have observed the dispersion of the quadratic EO component  $R_{11}$  in the off-resonant region, which is a clear advantage compared to other techniques like the quadratic electroabsorption technique [18], [19], where measurements are only possible in the resonant region. Compared to our proposed technique, the modified Teng-Man technique [29], [30] has the disadvantage that the quadratic EO signal is near to the detection limit. Besides that, the proposed technique gives for the first time valuable information about the in-device performance of the polymer in terms of the dispersion of the quadratic EO effect. This cannot be achieved by more traditional techniques like the prism coupling technique [31] since the lowest film thickness in this case is given by  $\lambda/2$  due to the measurement principle.

## 5. Conclusion

We present a benchmarking procedure to determine the dominant third-order susceptibility tensor components of linear conjugated NLO dyes that entail in-device dispersion measurements. The proposed technique allows to measure the quadratic EO component  $R_{11}$  of a conjugated polymer directly on-chip. Measurements are exemplified for a DR1/PMMA guest-host system. From that measurement we deduced the dispersion of  $R_{11}$  and evaluated  $R_{12}$  for the optical C- and O-band. This evaluation is possible under the assumption of a two-level model and that electronic

mechanisms are dominating in the off-resonant region. The present method enables not only to determine material properties in order to improve the device performance, but also for extending applications to different wavelengths.

## Acknowledgment

The authors would like to thank the valuable discussions with F. De Matteis from University of Rome “Tor Vergata.”

---

## References

- [1] S. Wolf *et al.*, “Coherent modulation up to 100 gbd 16qam using silicon-organic hybrid (soh) devices,” *Opt. Exp.*, vol. 26, no. 1, pp. 220–232, Jan. 2018. [Online]. Available: <http://www.opticsexpress.org/abstract.cfm?URI=oe-26-1-220>
- [2] S. Wolf *et al.*, “Silicon-organic hybrid (SOH) mach-zehnder modulators for 100 gbit/s on-off keying,” *Sci. Rep.*, vol. 8, no. 1, 2018, Art. no. 2598.
- [3] J. Leuthold *et al.*, “Silicon-organic hybrid electro-optical devices,” *IEEE J. Sel. Topics Quantum Electron.*, vol. 19, no. 6, pp. 114–126, Nov. 2013.
- [4] P. Steglich *et al.*, “Partially slotted silicon ring resonator covered with electro-optical polymer,” *Proc. SPIE*, vol. 9891, 2016, Art. no. 98 910R.
- [5] W. Heni *et al.*, “Silicon–organic and plasmonic–organic hybrid photonics,” *ACS Photon.*, vol. 4, no. 7, pp. 1576–1590, 2017.
- [6] H. Zwickel *et al.*, “Silicon-organic hybrid (SOH) modulators for intensity-modulation/direct-detection links with line rates of up to 120 gbit/s,” *Opt. Exp.*, vol. 25, no. 20, pp. 23 784–23 800, Oct. 2017. [Online]. Available: <http://www.opticsexpress.org/abstract.cfm?URI=oe-25-20-23784>
- [7] R. Palmer *et al.*, “Low power mach-zehnder modulator in silicon-organic hybrid technology,” *IEEE Photon. Technol. Lett.*, vol. 25, no. 13, pp. 1226–1229, Jul. 2013.
- [8] W. Heni *et al.*, “Nonlinearities of organic electro-optic materials in nanoscale slots and implications for the optimum modulator design,” *Opt. Exp.*, vol. 25, no. 3, pp. 2627–2653, Feb. 2017. [Online]. Available: <http://www.opticsexpress.org/abstract.cfm?URI=oe-25-3-2627>
- [9] F. Michelotti, E. Toussaere, R. Levenson, J. Liang, and J. Zyss, “Study of the orientational relaxation dynamics in a nonlinear optical copolymer by means of a pole and probe technique,” *J. Appl. Phys.*, vol. 80, no. 3, pp. 1773–1778, 1996. [Online]. Available: <https://doi.org/10.1063/1.362987>
- [10] A. Belardini, “Fluorinated and non-fluorinated electro-optic copolymers: Determination of the time and temperature stability of the induced electro-optic coefficient,” *Appl. Sci.*, vol. 2, no. 4, pp. 682–708, 2012. [Online]. Available: <http://www.mdpi.com/2076-3417/2/4/682>
- [11] H. Yu, L. Chen, K. Li, and X. Deng, “Electro-optic polymer waveguide modulator based on the pockels and kerr effects,” *Opt. Eng.*, vol. 52, 2013, Art. no. 044601. [Online]. Available: <https://doi.org/10.1117/1.OE.52.4.044601>
- [12] M. Qasymeh, M. Cada, and S. A. Ponomarenko, “Quadratic electro-optic kerr effect: Applications to photonic devices,” *IEEE J. Quantum Electron.*, vol. 44, no. 8, pp. 740–746, Aug. 2008.
- [13] P. Steglich *et al.*, “Quadratic electro-optic effect in silicon-organic hybrid slot-waveguides,” *Opt. Lett.*, vol. 43, no. 15, pp. 3598–3601, Aug. 2018. [Online]. Available: <http://ol.osa.org/abstract.cfm?URI=ol-43-15-3598>
- [14] P. Steglich *et al.*, “Quadratic electro-optical silicon-organic hybrid RF modulator in a photonic integrated circuit technology,” in *Proc. IEEE Int. Electron. Devices Meeting*, Dec. 2018, pp. 23.3.1–23.3.4.
- [15] B. Robinson *et al.*, “Optimization of plasmonic-organic hybrid electro-optics,” *J. Lightw. Technol.*, vol. 36, no. 21, pp. 5036–5047, Nov. 2018.
- [16] A. Messner *et al.*, “Plasmonic ferroelectric modulators,” *J. Lightw. Technol.*, vol. 37, no. 2, pp. 281–290, Jan. 2019.
- [17] M. G. Kuzyk, J. E. Sohn, and C. W. Dirk, “Mechanisms of quadratic electro-optic modulation of dye-doped polymer systems,” *J. Opt. Soc. Amer. B*, vol. 7, no. 5, pp. 842–858, May 1990. [Online]. Available: <http://josab.osa.org/abstract.cfm?URI=josab-7-5-842>
- [18] C. Poga, M. G. Kuzyk, and C. W. Dirk, “Quadratic electroabsorption studies of third-order susceptibility mechanisms in dye-doped polymers,” *J. Opt. Soc. Amer. B*, vol. 11, no. 1, pp. 80–91, Jan. 1994. [Online]. Available: <http://josab.osa.org/abstract.cfm?URI=josab-11-1-80>
- [19] C. Poga, T. M. Brown, M. G. Kuzyk, and C. W. Dirk, “Characterization of the excited states of a squaraine molecule with quadratic electroabsorption spectroscopy,” *J. Opt. Soc. Amer. B*, vol. 12, no. 4, pp. 531–543, Apr. 1995. [Online]. Available: <http://josab.osa.org/abstract.cfm?URI=josab-12-4-531>
- [20] J. Pérez-Moreno, S.-T. Hung, M. G. Kuzyk, J. Zhou, S. K. Ramini, and K. Clays, “Experimental verification of a self-consistent theory of the first-, second-, and third-order (non)linear optical response,” *Phys. Rev. A*, vol. 84, Sep. 2011, Art. no. 033837. [Online]. Available: <https://link.aps.org/doi/10.1103/PhysRevA.84.033837>
- [21] X. Zheng *et al.*, “The dispersion measurement of quadratic electrooptic effect of a linear conjugated polymer,” *IEEE J. Quantum Electron.*, vol. 45, no. 5, pp. 542–546, May 2009.
- [22] D. Knoll *et al.*, “High-performance photonic bimcos process for the fabrication of high-bandwidth electronic-photonic integrated circuits,” in *Proc. IEEE Int. Electron. Devices Meeting*, Dec. 2015, pp. 15.6.1–15.6.4.
- [23] P. Steglich *et al.*, “Novel ring resonator combining strong field confinement with high optical quality factor,” *IEEE Photon. Technol. Lett.*, vol. 27, no. 20, pp. 2197–2200, Oct. 2015.
- [24] P. Steglich *et al.*, “Hybrid-waveguide ring resonator for biochemical sensing,” *IEEE Sensors J.*, vol. 17, no. 15, pp. 4781–4790, Aug. 2017.

- [25] P. Steglich, C. Villringer, S. Dümecke, Y. P. Michel, M. Casalboni, and S. Schrader, "Silicon-on-insulator slot-waveguide design trade-offs," in *PHOTOPHOTICS 2015*, vol. 2, P. A. Ribeiro and M. Raposo, Eds. Setbal, Portugal: SCITEPRESS, Mar. 2015, pp. 47–52. [Online]. Available: <http://www.scitepress.org/DigitalLibrary/Link.aspx?doi=10.5220/0005336200470052>
- [26] P. Steglich, "Silicon-on-insulator slot waveguides: Theory and applications in electro-optics and optical sensing," in *Emerging Waveguide Technology*, K. Y. You, Ed. Rijeka, Croatia: IntechOpen, 2018, ch. 10. [Online]. Available: <https://doi.org/10.5772/intechopen.75539>
- [27] P. Steglich, C. Villringer, S. Pulwer, M. Casalboni, and S. Schrader, "Design optimization of silicon-on-insulator slot-waveguides for electro-optical modulators and biosensors," in *Photophotics 2015*. Berlin, Germany: Springer, 2016, pp. 173–187.
- [28] S. Bondarenko, C. Villringer, and P. Steglich, "Comparative study of nano-slot silicon waveguides covered by dye doped and undoped polymer cladding," *Appl. Sci.*, vol. 9, no. 1, 2018. [Online]. Available: <http://www.mdpi.com/2076-3417/9/1/89>
- [29] F. Michelotti, G. Nicolao, F. Tesi, and M. Bertolotti, "On the measurement of the electro-optic properties of poled side-chain copolymer films with a modified teng-men technique," *Chemical Phys.*, vol. 245, no. 1, pp. 311–326, 1999. [Online]. Available: <http://www.sciencedirect.com/science/article/pii/S0301010499001500>
- [30] M. Herold, W. Schmid, T. Vogtmann, R. Fischer, D. Haarer, and M. Schwoerer, "Electro-optic pockels and kerr effects for the determination of  $\chi(2)$  and  $\chi(3)$ : Thin films of side-chain polymers containing dimethylaminonitrostilbene and of the polydiacetylene poly-(butoxycarbonylmethyleneurethane)," *Appl. Opt.*, vol. 34, no. 6, pp. 996–1002, Feb. 1995. [Online]. Available: <http://ao.osa.org/abstract.cfm?URI=ao-34-6-996>
- [31] J. Zhou *et al.*, "Determination of dc kerr coefficients of polymer films with prism-optical waveguide configuration," *Appl. Phys. Lett.*, vol. 88, no. 2, 2006, Art. no. 021106.